Calibration of atomic-force microscope tips

Jeffrey L. Hutter, and John Bechhoefer

Citation: Review of Scientific Instruments **64**, 1868 (1993);
View online: https://doi.org/10.1063/1.1143970
View Table of Contents: http://aip.scitation.org/toc/rsi/64/7
Published by the American Institute of Physics

Calibration of atomic-force microscope tips

Jeffrey L. Hutter and John Bechhoefer
Department of Physics, Simon Fraser University, Burnaby, British Columbia, V5A 1S6, Canada

(Received 29 March 1993; accepted for publication 12 April 1993)

Images and force measurements taken by an atomic-force microscope (AFM) depend greatly on the properties of the spring and tip used to probe the sample's surface. In this article, we describe a simple, nondestructive procedure for measuring the force constant, resonant frequency, and quality factor of an AFM cantilever spring and the effective radius of curvature of an AFM tip. Our procedure uses the AFM itself and does not require additional equipment.

I. INTRODUCTION

Since its invention in 1986, the atomic-force microscope[1] (AFM) has become an increasingly important tool for studying surfaces at the atomic level. Beyond the often spectacular and occasionally informative images obtained of surfaces, the AFM has the potential to give quantitative information about *local* forces and interactions.[2–6] The accuracy of such measurements depends upon a knowledge of the physical properties of the spring and tip that probe these forces. In particular, one needs estimates of the size of the tip and the force constant of the cantilever spring to which the tip is attached.

Despite this need for calibration of individual tips and cantilevers, measurements of these properties have either been based on theoretical estimates or have been made only on supposedly representative samples. Typically, the radius of an AFM tip is taken from manufacturer's specifications or, rarely, measured by electron microscopy.[7–9] In the former case one uses a nominal figure that represents an average for a batch of microfabricated tips, while, in the latter, measurements are difficult and are likely to destroy the tip.[10] In either case, only the average macroscopic radius of curvature will be measured. However, the tip-sample interaction is dominated by the small portion of the tip closest to the sample. Since the tip is not likely to end in a perfect sphere, particularly in the case of pyramidal tips, such an average value will not serve as a very useful calibration.

Similarly, the force constants of cantilevers are rarely measured;[10a] rather, they are inferred from theoretical estimates based on the geometry and elastic properties of the cantilevers.[11] Often, the calculations themselves are suspect, since they are generally based on a simple, rectangular-beam geometry while the actual springs are "V" shaped. In addition, the cantilevers are often made of several materials (e.g., gold on silicon nitride), making a proper estimate of their elastic properties difficult. More important, this approach neglects the possibility of variation in the force constants of individual springs due to structural defects and variations in the lever geometry and composition. For example, since the spring constant depends on the lever thickness t as t^3, even small variations in the thickness will result in large variations among the force constants of nominally identical springs. Also, tip and spring properties may change over time. One might wish to check, for example, whether a tip has been blunted after crashing into a sample surface.

In this article, we describe a nondestructive procedure for calibrating individual cantilevers and tips for use in atomic-force microscopy. In Sec. II, we review the two common AFM imaging modes. In Sec. III, we show that measurements of thermal fluctuations of the cantilever can yield its spring constant, resonant frequency, and the quality factor of the resonance. In Sec. IV, we show that measurements of van der Waals forces on the tip allow an effective tip radius to be inferred. In Sec. V, we present representative data from the calibration of a silicon-nitride cantilever with an integral pyramidal tip.

II. THE ATOMIC-FORCE MICROSCOPE

The AFM probes the surface of a sample by moving the sample beneath a tip attached to a weak cantilever spring while the tip is in contact, or near contact, with the surface. The sample is typically moved by piezoelectric scanners capable of accurate movement on subangstrom scales. The tip deflection can be measured with a resolution as small as 0.05 Å.

The AFM is operated in either of two modes. In the *contact mode*, the tip adheres to the sample surface with a finite force as it is dragged across the surface. The finite adhesion forces deform the tip and sample so that contact occurs over a finite area.[12,13] This area is greatly influenced by the tip sharpness and is increased by any additional spring force.

In the *attractive mode*, long-ranged van der Waals (vdW) forces deflect the tip, which is suspended 40–50 Å above the surface. The strength of the vdW interaction depends on the tip sharpness and the amount of spring deflection is fixed by the spring constant. For both imaging modes, the tip sharpness and cantilever spring constant must be known in order to interpret images quantitatively. In addition, the AFM has been used for force-versus-distance measurements, where these parameters are again required.

Estimates of both of these important probe parameters can be made by measuring the motion of a tip above a sample. We will model the experimental configuration as a spherical tip of radius R and mass m suspended a distance D above a flat sample by a spring force constant k, as shown in Fig. 1. If the tip is far from the sample, its motion

 0034-6748/93/64(7)/1868/6/$6.00

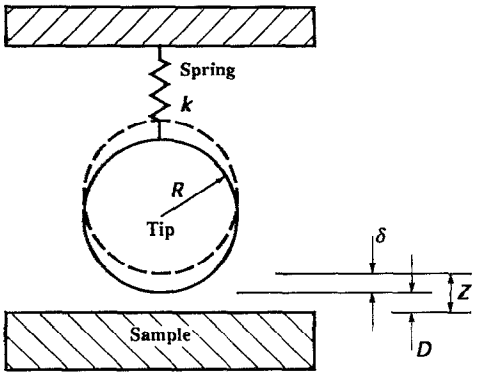

FIG. 1. Model of an AFM tip-sample system. In this model, a spherical tip of radius R is held at a distance D from a planar sample by a spring of force constant k. The tip-sample interaction causes a tip deflection of δ from a position a distance Z above the sample that the tip would occupy in the absence of any interactions.

is due only to thermal fluctuations. Measurements of this motion at frequencies near the resonant frequency of the spring allow one to estimate the spring constant. When the tip is closer to the sample, long-range forces will deflect it by some amount δ. If the nature and magnitude of these forces are known, the size of the tip may be deduced.

III. THERMAL FLUCTUATIONS

A harmonic oscillator in equilibrium with its surroundings will fluctuate in response to thermal noise. The Hamiltonian of such a system is

$$H=\frac{p^2}{2m}+\frac{1}{2}m\omega_0^2q^2, \tag{1}$$

where q is the displacement of the oscillator, p is its momentum, m is the oscillating mass, and ω_0 is the resonant angular frequency of the system. By the equipartition theorem, the average value of each quadratic term in the Hamiltonian is given by $k_BT/2$, where k_B is Boltzmann's constant and T is the temperature. In particular,

$$\langle\tfrac{1}{2}m\omega_0^2q^2\rangle=\tfrac{1}{2}k_BT. \tag{2}$$

As $\omega_0^2=k/m$, the force constant may be obtained from a measurement of the mean-square spring displacement as

$$k=k_BT/\langle q^2\rangle. \tag{3}$$

For a spring constant of 0.05 N/m, typical of relatively weak AFM cantilevers, thermal fluctuations will be of the order of 3 Å at room temperature. For such small deflections, we can approximate an AFM cantilever as a simple harmonic oscillator with one degree of freedom. (Other elastic modes of the cantilever have a much higher force constant and thus do not contribute much to the value of $\langle q^2\rangle$.) This would imply that if we measure the rms fluctuations of a freely moving cantilever with a sampling frequency much higher than its resonant frequency (to avoid averaging out the fluctuations), we can estimate the spring constant. However, other noise sources are present.

In order to isolate the contribution due to thermal oscillations, we examine the data in the frequency domain. In the absence of additional noise sources and in the limit of small damping, the power spectral density of the fluctuations in the spring displacement has a Lorentzian line shape.[14] Other noise sources add a background to this thermal response. As none of the other noise sources is likely to have a resonance at the resonant frequency of the cantilever, it is a simple matter to subtract this background. The area below the remaining peak is then a measure of the power of the cantilever fluctuations. Since the integral of the power spectrum equals the mean square of the fluctuations in the time-series data,[15] the estimate of the spring constant becomes

$$k=k_BT/P, \tag{4}$$

where P is the area of the power spectrum of the thermal fluctuations alone.

IV. TIP DEFLECTION

As the AFM tip is moved closer to the sample, the cantilever will deflect because of long-ranged tip-sample interactions. In the case of an AFM operated in air or vacuum with an electrically neutral sample, the only long-ranged force will be the van der Waals (vdW) attraction. The van der Waals potential between two molecules has the familiar $-C/r^6$ form. In order to calculate the vdW force between two macroscopic bodies, one may use a continuum approach and integrate the $1/r^6$ interaction over the two volumes.[16] For our case of a sphere interacting with a flat surface, the potential has the approximate form

$$W(D)=(AR/6D), \quad D\ll R, \tag{5}$$

where $A\equiv\pi^2C\rho_1\rho_2$ is the so-called Hamaker constant, and ρ_1 and ρ_2 are the densities of the two solids.

The potential energy for the AFM model described in Fig. 1 may be written as

$$E(\delta,Z)=-\frac{AR}{6(Z+\delta)}+\frac{1}{2}k\delta^2, \tag{6}$$

where Z, the distance between the surface and an imaginary undeflected tip, is determined by the piezo extension and acts as a control parameter. This energy function has a singularity at $\delta=-Z$ when the tip-sample distance is zero. Of course, contact forces always limit the approach distance to a few angstroms. The vdW force will deflect the spring to minimize the potential energy. Local minima of the energy function may be found by setting its derivative equal to zero:

$$\frac{dE(\delta,Z)}{d\delta}=\frac{AR}{6(Z+\delta)^2}+k\delta=0. \tag{7}$$

Thus, the critical values of E are the solutions of a cubic equation, allowing the tip deflection to be calculated analytically. Note that Eqs. (6) and (7) may be scaled so that they depend on only one parameter, $l\equiv\sqrt[3]{AR/k}$, which characterizes the length scale at which the vdW interaction is comparable to the spring potential.

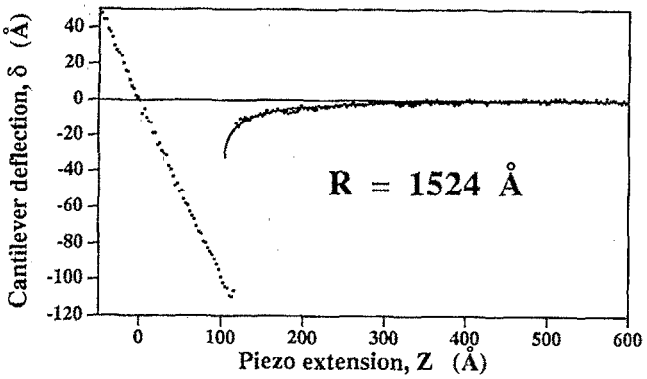

FIG. 2. Typical force spectrum showing the deflection of a cantilever as a function of sample displacement. The axes have been scaled so that the y axis records the deflection of the tip, while the x axis indicates the position of the sample relative to the point where the sample and tip would be in contact for an *undeflected* tip. During a force spectrum, the tip-sample separation is decreased from a relatively large value of Z (at a rate of 120 Å/s in this case). The solid curve is a fit of the theoretical tip-deflection to the data. Note that this curve extends to the left of the snapping point, indicating that fluctuations have caused the tip to snap in to contact with the sample at a distance greater than that predicted by our model.

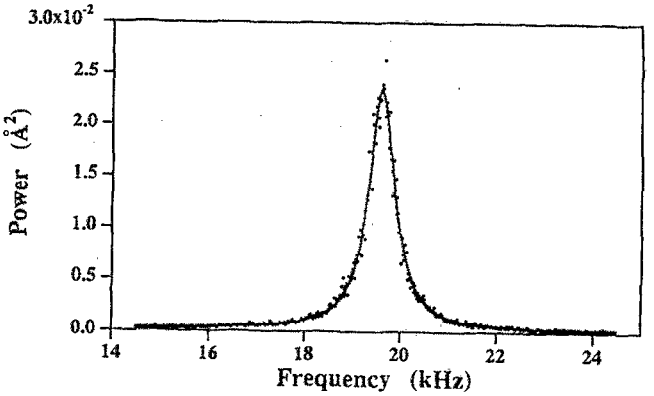

FIG. 3. Power spectral density plot of fluctuations in the output of the cantilever deflection detector. The plot is the average of six spectra of 5000 points each, binned into a 500 point curve. The resonant peak is fit to a Lorentzian.

For large tip-sample distances, the cantilever feels no forces and $\delta=0$. As Z is decreased, moving the tip and sample together, an attractive vdW interaction ($A>0$) causes the tip to be deflected toward the sample. Solving Eq. (7) for δ, we find that when Z is decreased to $Z_s=3^{2/3}l/2$, the magnitude of the gradient of the vdW force becomes larger than that of the spring force, so that the solution corresponding to the slightly deflected tip becomes unstable.[17] At this point, cantilever deflection will have brought the tip to a distance of $D^*=2Z_s/3=l/\sqrt[3]{3}$ from the sample. The tip must then "snap" into contact with the surface. For typical values of the Hamaker constant, tip radius, and spring constant ($A\sim10^{-19}$ J, $R\sim500$ Å, and $k\sim0.05$ N/m, respectively), the tip will jump into contact with the surface when it is about 46 Å away. This separation is still large enough that atomic-scale roughness will have a negligible effect on determining the tip deflection and snapping point. Note, too, that the tip-sample distance at the snapping point is considerably less than the tip radius, so that the assumption in Eq. (5) that $D\ll R$ in the region of interest is justified.

Values of the parameter l can be estimated by performing a "force spectrum" with the AFM. In a force spectrum, the sample is moved vertically and the resulting cantilever deflection is measured to generate a plot of δ vs Z. An example of such a curve is shown in Fig. 2. At long ranges, the tip is unaffected by the sample and moves with the thermal fluctuations of the cantilever. As the tip-sample distance is decreased, the vdW attraction causes the cantilever to deflect toward the surface until the tip snaps into contact. After this, the tip and sample move together: every angstrom the piezo is extended compresses the spring by one angstrom, as well. Eventually, the sample drives the cantilever back to its undeflected position, setting the zero point for the Z axis.

Experimental values of l can be obtained from a force spectrum by measuring the value of Z_s. In practice, thermal fluctuations and mechanical vibration allow the tip to overcome the energy barrier to snapping before the critical value of Z is reached. Given an approach speed and assuming that only thermal fluctuations are relevant, one can estimate the distance at which the instability actually occurs. The calculation is formally equivalent to the one done by Kramers for the tunneling rate of a particle over a potential barrier (in the small-viscosity limit).[18] The result is that the correction is large if one measures the discontinuity using the tip deflection (i.e., measures along the y axis of Fig. 2) and small if one measures the piezo displacement (i.e., measures along the x axis of Fig. 2). This is consistent with the plot of the full theoretical curve in Fig. 2. To avoid the uncertainties due to variation in the snapping distance from run to run, we decided to fit to the tip deflection *before* the instability. This yielded consistent results. The value of l allows us to calculate an experimental value of R, provided that we have measured the force constant and have an estimate of the Hamaker constant.[19] Details of the calculations of Hamaker constants have been included in Appendix A.

V. A SAMPLE CALIBRATION

The method of tip calibration detailed above has been applied to microfabricated Si_3N_4 cantilevers with integral pyramidal tips.[20] Typical results are discussed below.

Figure 3 shows the power spectrum of the fluctuations in the displacement of a typical spring. In our case, the analog-to-digital converter of the AFM electronics was unable to measure useful time-series data owing to a combination of a low signal-strength and low resolution. Instead, we used a lock-in amplifier[21] to measure the deflection-detector signal-power as a function of frequency.[22] The y axis of this figure has units of Å^2, which is appropriate for a power spectral density of displacement fluctuations. To calibrate the detector signal in terms of tip displacement, we needed first to measure the displacement of the piezoelectric tube scanner as a function of applied voltage. Since several schemes for calibrating the piezo have already been

published,[23] we leave the details of our method to Appendix B. Essentially, a linear variable differential transformer (LVDT) displacement sensor was used to measure the piezo scanner response. The detector could be calibrated once the piezo response was known by using the measurement of cantilever deflection in those portions of the force spectra where the tip and sample were in contact. Note that the deflection detector is calibrated in terms of vertical piezo displacement while the cantilever is tilted about 15° from the vertical. The scale of Fig. 3 has been corrected so that fluctuations are measured in a direction normal to the cantilever plane.

In addition to the thermal fluctuations of the cantilever, background instrumental noise must be subtracted from the spectrum. Over the frequency range shown in Fig. 3, the noise spectrum is flat. At low frequencies, $1/f$ noise becomes important so that a direct measurement of $x(t)$ that does not filter low frequencies would underestimate the true spring constant. The resonant peak is fit to a Lorentzian. Integrating this curve (with the background subtracted), we find the force constant of the cantilever to be $k=0.0167\pm0.0008$ N/m, where most of the uncertainty is in the calibration of the deflection detector. This result does not agree with the nominal value of 0.064 N/m claimed by the manufacturer. The resonant frequency for the cantilever, measured to be 19.6 kHz, is also quite far from its nominal value of 17 kHz. The quality factor of the cantilever resonance is calculated from the fit parameters to be $Q=30$.

A typical force spectrum for a mica sample is shown in Fig. 2. Both the piezo displacement (x axis) and detector output (y axis) have been calibrated[24] (see Appendix B). The deflection of the cantilever and eventual snap to contact are evident in this plot. The experimental data is fit to a theoretical model of the tip deflection in the region before the snap. Note that the model curve given by the best fit extends below the experimental value of Z_s, indicating that the snap has occurred at a distance greater than that predicted by the model. For our tip, averaging values obtained from more than twenty force spectra resulted in an estimate of the effective tip radius of $R=1500\pm160$ Å (using the value of A calculated in Appendix A). Most of the uncertainty in this figure is in the Hamaker constant and spring constant—the statistical uncertainty in the range of values obtained from the individual fits was only 2%.[25] The nominal macroscopic radius of curvature for the batch of tips used was 400 Å.[26] A possible explanation for this large effective radius is that a microfabricated pyramidal tip may terminate in a line rather than an point if the base of the tip is not perfectly square. The effective radius would then depend on both the rounding of the tip along this line and the length of the line. It is also possible that some irreversible deformation of the tip occurred while it was in contact with the sample. We emphasize that, far from being a detail, such information about the tip is crucial in interpreting images and force measurements.

VI. DISCUSSION

We have described a simple calibration procedure for AFM tips whose essential steps can be implemented using the hardware available with any AFM. This calibration is particularly useful when the tip is to be used for force measurements. However, it may also aid in tip selection when maximum resolution (minimum R) or a particular cantilever stiffness is required.

Our own work that motivated this study has focused on the measurement of Hamaker constants for the silicon nitride-mica system immersed in various liquids. We have shown that even when van der Waals forces are very weak, the snapping distance of the tip-deflection curve can yield quantitative estimates of the Hamaker constant—once the tip radius and spring constant have been calibrated.[6]

ACKNOWLEDGMENTS

This study was supported by NSERC operating and equipment grants. J.B. is an Alfred P. Sloan Fellow.

APPENDIX A: THE HAMAKER CONSTANT

The expression for the Hamaker constant in terms of the vdW force constant C given in Sec. IV ignores many-body effects and retardation effects for large distances. Many-body effects do not alter the form of the interaction potential; they only change the value of the Hamaker constant. In the nonretarded limit, the Hamaker constant between two media can be calculated using the Lifshitz theory.[27] According to this approach, the Hamaker constant depends on the dielectric responses, $\epsilon(\omega)$, of the two media involved and is given by[28]

$$A_{12}=\frac{3k_BT}{2}\sum_{n=0}^{\infty'}\sum_{s=1}^{\infty}\frac{(\Delta_{1;n}\Delta_{2;n})^s}{s^3}, \tag{A1a}$$

where

$$\Delta_{j;n}=\frac{\epsilon_j(i\xi_n)-1}{\epsilon_j(i\xi_n)+1}, \tag{A1b}$$

and

$$\xi_n=n(2\pi k_BT/\hbar), \tag{A1c}$$

and where the prime on the first summation indicates that the $n=0$ term is given half weight. The numerical subscripts on A and Δ refer to the tip (1) and sample (2). The formulas are slightly more complicated when the intervening medium is a liquid, rather than air or vacuum.) The Hamaker constant, then, depends on the dielectric properties of the media via the dielectric functions evaluated at complex frequencies. These $\epsilon(i\xi)$ functions are, however, real functions and can be evaluated through the Kramers–Kronig relation[29]

$$\epsilon(i\xi)=1+\frac{2}{\pi}\int_0^{\infty}\frac{\omega\epsilon''(\omega)}{\omega^2+\xi^2}\,d\omega. \tag{A2}$$

In this expression, $\epsilon''(\omega)$ is the imaginary part of the dielectric response and is proportional to the absorption at frequency ω. As can be seen, the $\epsilon(i\xi)$ function is real and

TABLE I. Dielectric data for tip and sample materials.

Medium	C_{IR}	ω_{IR} ($\times 10^{14}$ s^{-1})	C_{UV}	ω_{UV} ($\times 10^{16}$ s^{-1})
Si_3N_4[a]	2.558	4.008	2.782	1.303
Mica[b]	3.917	1.884	1.483	1.57

[a]Values derived from data in Ref. 35.
[b]Values from Ref. 36.

decreases monotonically in ξ (from ϵ_0 at $\xi=0$ to a value of 1 as $\xi\to\infty$). Furthermore, it is constant in frequency ranges where the absorption ϵ'' is zero. Armed with a knowledge of the absorption spectra of the media, we can calculate the vdW interactions between the tip and the sample. However, we must remember that our numerical estimates will only be as good as the dielectric data used to compute the $\epsilon(i\xi)$ function.

To calculate Hamaker constants, we need an explicit representation of the functions $\epsilon(i\xi)$ for each of the materials involved. In principle, this would require measuring the absorption spectrum for all frequencies, which is impractical. However, Ninham and Parsegian[30] have shown that $\epsilon(i\xi)$ for insulators can be adequately approximated by functions of the form

$$\epsilon(i\xi)=1+\sum_{i=1}^{N}\frac{C_i}{1+(\xi/\omega_i)^2}. \tag{A3}$$

They assume that there are N absorptions with strengths C_i in narrow frequency bands located at frequencies ω_i. For most purposes, it is sufficient to consider only a single infrared (IR) and a single ultraviolet (UV) absorption, which account for vibrational and electron ionization absorption, respectively. The IR and UV absorptions can be inferred from the static dielectric constant ϵ_0 and $n(\omega)$ data for each medium.[28]

Any flat, electrically neutral sample is suitable for tip calibrations if dielectric data for the material are available. Experimentally, graphite provides good results, but theoretical estimates of $\epsilon(i\xi)$ are less accurate for conductors than they are for insulators. We chose instead to use a cleaved muscovite mica surface, though care must be taken in the preparation of the sample. Since the mica surface usually becomes charged when cleaved, best results are obtained when the ambient humidity is high enough to discharge the surface. On the other hand, if the humidity is too high, water condenses between tip and sample, and surface-tension forces dominate. In practice, good results were obtained when the ambient humidity was between 40% and 70%. Samples cleaved in air that was too dry could be discharged by setting a beaker full of water next to the mica. Since both electrostatic and capillary forces have a range of order 1 μm or more, it was easy to check whether either was present: in good samples, there was no measurable tip deflection until the tip was less than 200 Å from the surface. Note, finally, that the monolayer of water that collects on the mica surface will not measurably affect the value of A.

Using the dielectric data listed in Table I, we estimate the Hamaker constant for a Si_3N_4-air-mica system to be $(1.1\pm0.1)\times10^{-19}$ J.

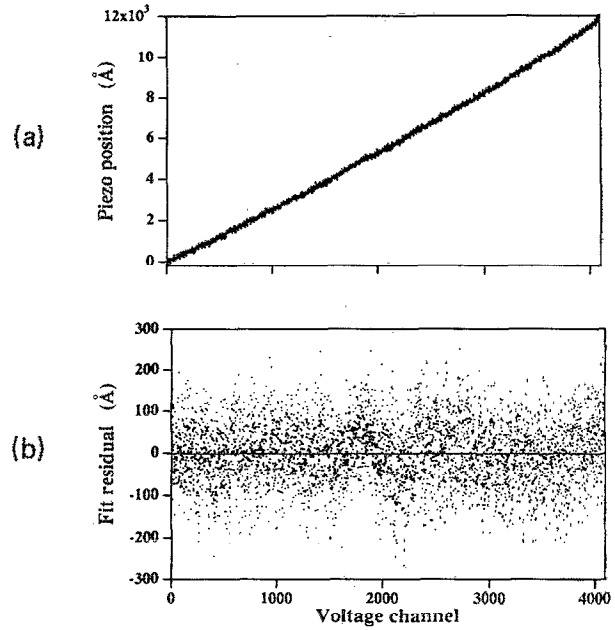

FIG. 4. Measurement of the piezo displacement as a function of the applied voltage in terms of the binary channel set by the AFM control unit. (a) Displacement of the piezo measured by an LVDT. (b) Residuals of a quadratic fit to the data.

APPENDIX B: CALIBRATION OF THE AFM

One of the difficulties in the cantilever calibration procedure described in this article is that both the vertical motion of the piezoelectric tube scanner and the sensitivity of the deflection detector must be accurately calibrated. The piezo response and detector sensitivity are, in general, nonlinear and both responses are folded into the single measurement of tip deflection. The nonlinearity is small enough that both the piezo and detector responses can be considered to be linear in the region of interest, which is of the order of 100 Å in extent—a small portion of the available scanning range for the piezo and deflection range for the tip. Below, we describe a procedure to calibrate both the piezo and the detector of an AFM.

1. Piezo calibration

The scanner tubes are usually calibrated by the manufacturer, but we found that calibration parameters can change over time. In order to obtain an accurate expression for the piezo response prior to cantilever calibrations, a linear variable differential transformer (LVDT) displacement transducer[31] was used to measure the piezo position over its full vertical range. The piezo range was approximately one μm in our case, which is a small displacement, even for relatively sensitive LVDTs. However, an adequate calibration was obtained by averaging several sets of data, each of which consisted of 4096 calibration points.[32]

The piezo calibration is shown in Fig. 4(a) where fifteen separate runs were averaged. The y axis of this plot was calibrated in units of angstroms using the LVDT

(which was itself calibrated using a micrometer). The x axis is recorded in units corresponding to the digitized voltage output from the AFM control module to the piezo. This curve is accurately modeled as a quadratic, as the fit residuals show in Fig. 4(b). The resulting expression for the piezo displacement as a function of binary voltage channel was then used to calibrate the displacement scale in measured force spectra.

2. Detector calibration

Several methods of detecting cantilever deflection are in use. In our case, cantilever deflection is measured using the optical-lever technique.[33] In this detection system, a laser beam is reflected from the back of the cantilever onto a position-sensitive photodetector (PSPD). The cantilever deflection is then measured as a difference signal between the two halves of the PSPD. This signal is not likely to be linear with the deflection; rather, it depends on the cross-sectional intensity distribution of the reflected laser beam, which will be different each time the laser is adjusted for a new microlever.

Once the vertical response of the piezo scanner has been calibrated, we can calibrate the detector using part of the force-spectrum curve. This method is applicable to any detector system and can be done at the same time as the measurements for the snapping-distance calibration. If we assume that the compliance of the weak cantilever is smaller than that of either the tip or the sample,[34] then the deflection of the tip and the displacement of the sample must be equal once the two are in contact. This allows us to use the regions of force spectra where the tip and sample are in contact as calibration curves for the detector. As we only need to calibrate the detector for deflections smaller than a few nanometers, we can use a linear fit to a small portion of the force spectrum.

[1] G. Binnig and C. F. Quate, Phys. Rev. Lett. **56**, 930 (1986).
[2] Y. Martin, C. C. Williams, and H. K. Wickramasinghe, J. Appl. Phys. **61**, 4723 (1987).
[3] A. L. Weisenhorn, P. Maivald, H.-J. Butt, and P. K. Hansma, Phys. Rev. B **45**, 11 226 (1992).
[4] W. A. Ducker, T. J. Senden, and R. M. Pashley, Langmuir **8**, 1831 (1992).
[5] L. Olsson, P. Tengvall, R. Wigren, and R. Erlandsson, Ultramicroscopy **42–44**, 73 (1992).
[6] J. L. Hutter and J. Bechhoefer (unpublished).
[7] T. R. Albrecht, S. Akamine, T. E. Carver, and C. F. Quate, J. Vac. Sci. Technol. A **8**, 3386 (1990).
[8] H. Kado, K. Yokoyama, and T. Tohda, Rev. Sci. Instrum. **63**, 3330 (1992).
[9] M. Fotino, Rev. Sci. Instrum. **64**, 159 (1993).
[10] S. Akamine and C. F. Quate, J. Vac. Sci. Technol. B **10**, 2307 (1992).
[10a] A method for measuring the spring constant of cantilevers, different from ours, has recently been published. See J. P. Cleveland, S. Manne, D. Bocek, and P. K. Hansma, Rev. Sci. Instrum. **64**, 403 (1993).
[11] D. Sarid and V. Elings, J. Vac. Sci. Technol. B **9**, 431 (1991).
[12] N. A. Burnham, D. D. Dominguez, R. L. Mowery, and R. J. Colton, Phys. Rev. Lett. **64**, 1931 (1990).
[13] J. L. Hutter and J. Bechhoefer, J. Appl. Phys. **73**, 4123 (1993).
[14] C. V. Heer, *Statistical Mechanics, Kinetic Theory, and Stochastic Processes* (Academic, New York, 1972), p. 431.
[15] W. H. Press, B. P. Flannery, S. A. Teukolsky, and W. T. Vetterling, *Numerical Recipes in FORTRAN* (Cambridge University Press, Cambridge, 1989), Chap. 12.
[16] H. C. Hamaker, Physica **4**, 1058 (1937).
[17] D. Tabor and R. H. S. Winterton, Proc. R. Soc. London, Ser. A **312**, 435 (1969).
[18] For discussions of the Kramers problem, see H. A. Kramers, Physica **7**, 284 (1940), and P. Hänggi, P. Talkner, and M. Borkovec, Rev. Mod. Phys. **62**, 251 (1990).
[19] F. J. Giessibl and G. Binnig have also used measurements of tip deflection to model tip shape. F. J. Giessibl and G. Binnig (unpublished).
[20] The AFM and tips were purchased from Park Scientific Instruments (1171 Borregas Ave., Sunnyvale, CA 94089). The software controlling the force-spectrum routine was modified to acquire 4096 points per measurement. Note that, as delivered, the feedback circuit controlling vertical displacement of the piezoelectric tube scanner cannot be disabled. The result is that the voltage applied across the piezo differs from the imposed value by about one volt (over a range of 300 V full scale). The extra, uncontrollable voltage may be removed by grounding the appropriate "fast feedback" line of the DB25 connector joining the SFM probe module to the main control unit. We thank V. Croquette for alerting us to this peculiarity of the Park AFM.
[21] Model SR 850 DSP, Stanford Research Systems, 1290-D Reamwood Avenue, Sunnyvale, California 94089. Note that in order to measure quantitative power spectra using a lock-in amplifier, one must divide the apparent power by the equivalent-noise bandwidth of the lock-in.
[22] The lock-in was used more out of convenience than necessity. Further amplification of the detector signal would have permitted a direct measurement of the spring deflection.
[23] Y. Li and S. M. Linday, Rev. Sci. Instrum. **62**, 2630 (1991).
[24] In practice, the detector signal drifts slightly during the measurement. We correct for this drift by a linear subtraction that straightens the baseline. Once the instrumental drift was removed, we fit the data using a nonretarded vdW potential. This is justified because almost all of the measurable deflection occurs within 200 Å of the tip.
[25] The accuracy of our force spectrum measurements was increased—at the cost of measurement speed—by using a good voltmeter to measure directly the detector signal.
[26] Had our measurement of the spring constant agreed with the manufacturer's estimate, our value for the tip radius would have *increased* by a factor of 4.
[27] E. M. Lifshitz, Sov. Phys. JETP **2**, 73 (1956).
[28] D. B. Hough and L. R. White, Adv. Colloid. Interface Sci. **14**, 3 (1980).
[29] L. D. Landau and E. M. Lifshitz, *Electrodynamics of Continuous Media* (Pergamon, New York, 1960).
[30] B. W. Ninham and V. A. Parsegian, Biophys. J. **10**, 646 (1970).
[31] Lucas Schaevitz, 7905 N. Route 130, Pennsauken, NJ 08110-1489.
[32] Note that the most recent versions of the AFM have tended to incorporate integral systems to measure and control piezo displacement. For such AFM's, this part of our calibration is obviously unnecessary.
[33] G. Meyer and N. M. Amer, Appl. Phys. Lett. **53**, 1045 (1988).
[34] S. J. O'Shea and M. E. Welland, Appl. Phys. Lett. **60**, 2356 (1992).
[35] *Handbook of Optical Constants of Solids*, edited by E. D. Palik (Academic, Orlando, 1985).
[36] J. Mahanty and B. W. Ninham, *Dispersion Forces* (Academic, New York, 1976), p. 74.